

## Noncontact monitoring of respiratory rate in newborn infants using thermal imaging

Pereira, Carina Barbosa; Yu, Xinchu; Goos, Tom; Reiss, Irwin; Orlikowsky, Thorsten; Heimann, Konrad; Venema, Boudewijn; Blazek, Vladimir; Leonhardt, Steffen; Teichmann, Daniel

**DOI**

[10.1109/TBME.2018.2866878](https://doi.org/10.1109/TBME.2018.2866878)

**Publication date**

2019

**Document Version**

Final published version

**Published in**

IEEE Transactions on Biomedical Engineering

**Citation (APA)**

Pereira, C. B., Yu, X., Goos, T., Reiss, I., Orlikowsky, T., Heimann, K., Venema, B., Blazek, V., Leonhardt, S., & Teichmann, D. (2019). Noncontact monitoring of respiratory rate in newborn infants using thermal imaging. *IEEE Transactions on Biomedical Engineering*, *66*(4), 1105-1114.  
<https://doi.org/10.1109/TBME.2018.2866878>

**Important note**

To cite this publication, please use the final published version (if applicable).  
Please check the document version above.

**Copyright**

Other than for strictly personal use, it is not permitted to download, forward or distribute the text or part of it, without the consent of the author(s) and/or copyright holder(s), unless the work is under an open content license such as Creative Commons.

**Takedown policy**

Please contact us and provide details if you believe this document breaches copyrights.  
We will remove access to the work immediately and investigate your claim.

# Noncontact Monitoring of Respiratory Rate in Newborn Infants Using Thermal Imaging

Carina Barbosa Pereira<sup>1</sup>, Xinchu Yu, *Student Member, IEEE*, Tom Goos<sup>2</sup>, Irwin Reiss, Thorsten Orlikowsky, Konrad Heimann, Boudewijn Venema<sup>3</sup>, Vladimir Blazek, Steffen Leonhardt<sup>4</sup>, *Senior Member, IEEE*, and Daniel Teichmann<sup>5</sup>, *Member, IEEE*

**Abstract**—Monitoring of respiratory rate (RR) is very important for patient assessment. In fact, it is considered one of the relevant vital parameters in critical care medicine. Nowadays, standard monitoring relies on obtrusive and invasive techniques, which require adhesive electrodes or sensors to be attached to the patient's body. Unfortunately, these procedures cause stress, pain, and frequently damage the vulnerable skin of preterm infants. This paper presents a “black-box” algorithm for remote monitoring of RR in thermal videos. “Black-box” in this context means that the algorithm does not rely on tracking of specific anatomic landmarks. Instead, it automatically distinguishes regions of interest in the video containing the respiratory signal from those containing only noise. To examine its performance and robustness during physiological (phase A) and pathological scenarios (phase B), a study on 12 healthy volunteers was carried out. After a successful validation on adults, a clinical study on eight newborn infants was conducted. A good agreement between estimated RR and ground truth was achieved. In the study involving adult volunteers, a mean root-mean-square error (RMSE) of  $(0.31 \pm 0.09)$  breaths/min and  $(3.27 \pm 0.72)$  breaths/min was obtained for phase A and phase B, respectively. In the study involving infants, the mean RMSE hovered around  $(4.15 \pm 1.44)$  breaths/min. In brief, this paper demonstrates that infrared thermography might become a clinically relevant alternative for the currently available RR monitoring modalities in neonatal care.

Manuscript received February 13, 2018; revised July 2, 2018; accepted August 14, 2018. Date of publication August 23, 2018; date of current version March 19, 2019. The work of C. B. Pereira was supported by the FCT (Foundation for Science and Technology in Portugal) under Ph.D. Grant SFRH / BD / 84357 / 2012. (Carina Barbosa Pereira and Xinchu Yu contributed equally to this work.) (*Corresponding author: Carina Barbosa Pereira.*)

C. B. Pereira is with the Chair for Medical Information Technology, RWTH Aachen University, Aachen 52074, Germany (e-mail: pereira@hia.rwth-aachen.de).

X. Yu, B. Venema, S. Leonhardt, and D. Teichmann are with the Chair for Medical Information Technology, RWTH Aachen University.

T. Goos is with the Department of Biomedical Engineering, Delft University of Technology and also with the Division of Neonatology, Department of Pediatrics, University Medical Center Rotterdam.

I. Reiss is with the Division of Neonatology, Department of Pediatrics, University Medical Center Rotterdam.

T. Orlikowsky and K. Heimann are with the Department of Neonatology, University Children's Hospital, University Hospital RWTH Aachen.

V. Blazek is with the Chair for Medical Information Technology, RWTH Aachen University and also with the Czech Institute of Informatics, Robotics and Cybernetics, CTU Prague.

Digital Object Identifier 10.1109/TBME.2018.2866878

**Index Terms**—Infrared thermography, thermal imaging, respiratory rate, remote monitoring, healthy subjects, newborn infants.

## I. INTRODUCTION

RESPIRATION is an important physiological process which ensures oxygen supply to the human body and removal of carbon dioxide from the circulation. Each respiratory cycle consists of two phases: inspiration of oxygen-rich air necessary for metabolism, and expiration of carbon dioxide generated during energy-producing reactions [1]. Thus, monitoring of respiratory function, and especially, respiratory rate (RR) is very important for patient assessment [2]–[4]. Indeed, RR is considered a crucial vital parameter in critical care medicine [3], [5].

Respiratory rate, usually measured in breaths per minute (breaths/min), describes the rate of the respiratory cycles. Normal values for this vital sign vary according to age. While RR of adults normally ranges between 12 to 20 breaths/min, RR of preterm infants may vary between 40 to 60 breaths/min [6].

Diverse diseases contribute to breathing disorders, which are commonly identified either by abnormal RRs, respiratory sounds, or by an atypical waveform (altered breathing depth and/or rhythm) [7]–[9]. Tachypnea (increased RR), for example, can be an early indicator for heart and lung diseases. Bradypnea (decreased RR), in turn, may be caused by hypothermia, certain medications (e.g. narcotics) or by diseases affecting the central nervous system [10]. Other pathological breathing patterns such as Kussmaul's breathing or Cheyne-Stokes respiration are commonly associated e.g. with cerebral ischemia [11], [12] and metabolic disorders [13]. In context with preterm neonates, the continuous surveillance of the respiratory rate and its variations is mandatory, since apneas and bradycardia occur frequently. If not detected early, they may lead to oxygen-depletion in the organs, resulting e.g. in deficits in their neurodevelopmental outcome [14]. Furthermore, tachypnea is one of the leading clinical signs for bacterial pulmonary infection [15]. Finally, this vital sign contributes to an early identification of sudden infant death syndrome, which is one of the major causes for death in children younger than one year [16].

However, RR is still one of the most clinically undocumented and underestimated vital signs, mostly due to shortcomings of current clinical monitoring techniques [3], [17]. These modalities rely on the attachment of sensors to the patients body, which

induce stress and discomfort [18]. In preterm and very low birth weight (VLBW) infants, placement and removal of adhesive electrodes frequently lead to epidermal stripping and skin disruption because the electrode-dermis junction is stronger than the bond between the epidermis and dermis. In fact, removal of adhesive electrodes is the major cause of skin breakdown in neonatal intensive care units (NICUs) [19], [20].

In recent years, there has been a great effort to develop non-contact RR monitoring techniques. Their major aim is to improve patients' quality of life [5]. One of the first techniques for contactless measurement of vital signs was the *Radar Vital Signs Monitor (RVSM)* developed by Greneker *et al.* in 1997 [21]. Steffen *et al.* [22] proposed in 2008 a multichannel simultaneous magnetic induction measurement system (MUSIMITOS) capable of monitoring heart and lung activity unobtrusively. In 2013, Marchionni *et al.* used a laser Doppler vibrometer, which measures vibrations of a surface, for contactless monitoring of respiration and heart rate in preterm infants [23]. Recently, the focus has broadened to encompass imaging technologies: visible and near-infrared [24]–[26], mid-wave infrared [16] as well as long wave infrared [27] imaging systems. Infrared thermography (IRT), also known as thermal imaging, is a very promising approach for unobtrusive and non-contact monitoring of both heart rate and RR [28]. In contrast to visible and near-infrared imaging systems, IRT does not require any active illumination. It is a completely passive technology which works in total darkness. Therefore, it is well suited for very sensitive patients such as neonates [29].

Most imaging approaches for RR monitoring [16], [30] including our previous works [27], [28], [31] are based on the detection and tracking of certain feature points or anatomic landmarks such as the nose. Abbas *et al.* [27] presented in 2011 an algorithm which estimated the RR using a continuous wavelet transform of the temperature modulation around the nostrils. The region of interest (ROI) was defined in the first frame and no tracking algorithm was used. They validated their approach using video data from seven premature infants. In 2017, our research group improved this approach by implementing a tracking algorithm. To estimate the instantaneous respiratory frequencies, three estimators were computed for each position of the short adaptive analysis window: *adaptive window autocorrelation*, *adaptive window average magnitude difference function*, and *adaptive maximum amplitude pairs* [32]. To the best of our knowledge, there aren't any other approaches in the literature, which use thermal imaging to monitor RR in infants. Further research groups (such as [16], [30]) tested their methods in video data from adult volunteers. Fei and co-authors [16] used a coalitional tracking algorithm to track motion. Posteriorly, the respiratory temperature waveform was normalized and wavelet analysis was applied to the re-sampled signal. Lewis *et al.* [30], in turn, tested a tracking method based on the Piecewise Bezier Volume Deformation model. The thermal signal, computed from both nostrils, was dynamically filtered and the breath interval was calculated using its first derivative.

The former techniques work well when the nose is clearly visible in the image, however they fail when the nose is outside the camera's field of view (patient lying on the side). In this paper,

we present a new “black-box” approach which does not rely on tracking of anatomic landmarks, but instead automatically detects respiration in image sequences.

For a proof-of-concept, the approach was firstly validated in a study involving healthy adult human subjects. Here, its ability to accurately measure RR during challenging conditions (simulated breathing disorders) was analyzed. A second study with newborn infants was performed at the division of Neonatology of the Sophia Children's Hospital (Erasmus MC, Rotterdam, The Netherlands); the aim was to evaluate the outcome of the algorithm in this particular group as well as in a clinical scenario.

In this paper, Section II presents the proposed algorithm. Section III describes the experimental protocol and setup of both studies. The results are presented in Section IV and discussed in Section V. Finally, Section VI concludes the paper and gives future perspectives.

## II. METHODOLOGY

In this paper, a “black-box” or grid-based approach was used. This means that instead of defining a ROI based on anatomic landmarks (e.g. the nose [16], [30]), a grid was laid over the image with each grid cell representing one ROI. The respiratory signal and RR were extracted for each ROI and afterwards analyzed with regard to its quality. Finally, suitable ROIs were automatically selected and information was fused in order to get robust estimations for RR. The above-mentioned steps are illustrated in Fig. 1 and are described below in detail. The algorithm was programmed and tested in MATLAB (MATLAB 2017a, The MathWorks Inc., Natick, MA, USA) using a 64-bit Windows 7 computer with a quad-core Intel® Corei™5-3450 3.10 GHz processor, 16 GB RAM and a solid-state drive. Data were analyzed offline.

### A. Extraction of Respiratory Signal and Estimation of Signal Quality

For the  $k$ th ROI, the signal  $s_{ROI_k}(t)$  at timestamp  $t$  was extracted by calculating the 2-dimensional mean value of all pixels within the ROI according to

$$s_{ROI_k}(t) = \frac{1}{mn} \sum_{i=0}^{m-1} \sum_{j=0}^{n-1} I_{ROI_k}(i, j, t). \quad (1)$$

The width and height of  $ROI_k$  are denoted by  $m$  and  $n$ , while  $I_{ROI_k}(i, j, t)$  denotes the intensity at pixel  $i, j$  at time stamp  $t$ . For further analysis, a hamming window was applied to the most recent 15 seconds of  $s_{ROI_k}(t)$ , resulting in the analysis window  $s_{w,ROI_k}(t)$ . As known, a rectangular window applied to a signal in the time domain can lead to distortions in the frequency domain. To minimize these distortions, a smoother window shape (Hamming window) was applied. When used, this de-emphasizes the edges and reduces their effects [33]. The length of 15 s was used because the resulting trade-off between time- (15 s) and frequency resolution (4 breaths/min) seemed reasonable to track changes in respiratory rate fast enough while maintaining sufficient accuracy. Posteriorly, the analysis

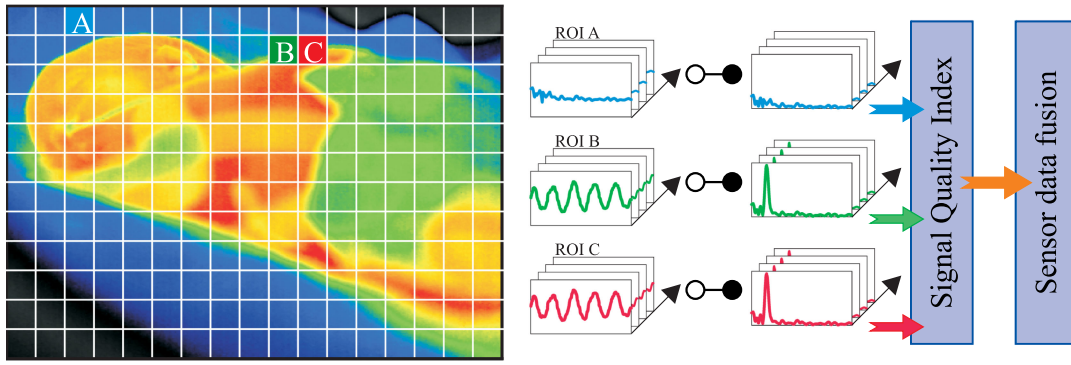


Fig. 1. Schematic representation of the major steps used to estimate RR.

window was mean centered and transformed into the frequency domain using a Fourier transform. Each window's spectrum  $S_{w,ROI_k}(f)$  was normalized to its maximum value.

In subsequent steps, three different frequency bands were considered:

- 1) Low-Pass (LP):  $f < 0.1 \text{ Hz}$ ,
- 2) Band-Pass (BP):  $0.1 \text{ Hz} \leq f \leq 3 \text{ Hz}$ ,
- 3) High-Pass (HP):  $f > 3 \text{ Hz}$ .

While the LP-Band contains low-frequency noise (e.g. baseline drift), the HP-Band contains high-frequency noise components (e.g. sensor noise or motion artefacts). The BP-Band is the frequency range of respiration. It ranges between 0.1 and 3 Hz in order to increase the number of applications of our approach. It can be used not only for monitoring RR in newborn infants (normal RR ranges between 40 and 60 breaths/min) but also for monitoring RR in adult patients (normal RR ranges between 12 and 20 breaths/min). Additionally, in the future, we plan to test the capability of the current approach to detect heart rate. The mean heart rate for adults ranges from 60 to 100 beats per minute (bpm) and that for preterm infants ranges from 120 to 170 bpm [6], [34], [35].

In order to determine whether the current analysis window of a ROI actually contains a respiration-related signal or only noise, a signal quality index (SQI) was empirically developed:

$$SQI = \begin{cases} 1 - [\frac{1}{2} \cdot F3 + \frac{1}{4} \cdot (F1 + F2)], & \text{if } F4 \geq 2 \\ 1 - \frac{1}{2} \cdot (F1 + F2), & \text{otherwise.} \end{cases} \quad (2)$$

It was based on four features (F1–F4) of the normalized spectrum, see Fig. 2. The first feature (F1) corresponds to the maximum within the HP-band. The second feature, F2, stands for the percentage of values in the HP-band larger than a given threshold. The third feature, F3, denotes the difference between maximum in the BP-band and maximum in the LP-band. The last feature, F4, refers to the ratio between the maximum in LP-band and maximum in BP-band.

The SQI takes both high frequency noise (features F1 and F2) as well as low frequency noise (features F3 and F4) into account. Due to its definition, possible values of the SQI are limited to  $[0, 1]$ . While a SQI of 1 indicates a very good signal quality, a SQI of 0 points towards a very poor signal quality.

## B. Selection of Grid Cells and Estimation of RR Using Information Fusion

For each ROI's current analysis window, the RR was defined as the frequency within the BP-Band with the maximum amplitude in the normalized spectrum. However, ROIs with an actual respiratory signal must be distinguished from those which do not contain a respiratory signal (e.g. background noise). This was accomplished by only accepting ROIs with a SQI higher than a threshold of 0.75, which was empirically defined. All other ROIs were excluded from further analysis.

Three different sensor fusion techniques were applied to the RRs of the ROIs  $RR_{ROI_k}$ , in order to estimate the instantaneous RR. The following paragraphs describe the three algorithms in detail.

**1) Median:** This first approach computes the median frequency of all valid ROIs. The fused RR ( $RR_t^{\text{fus}}$ ) at time point  $t$  is governed by the following equation:

$$RR_t^{\text{fus}} = 60 \cdot f_t^{\text{fus}}, \quad (3)$$

with

$$f_t^{\text{fus}} = \text{median}(f_t^i). \quad (4)$$

Here,  $f_t^{\text{fus}}$  stands for the fused frequencies at time point  $t$ . The variable  $f_t^i$  represents, in turn, the frequency at which the normalized power spectrum of the ROI  $k$  assumes its maximum:

$$f_t^i = \arg \max_{f_{\min} \leq f \leq f_{\max}} S_{ROI_k, \text{norm}}(f). \quad (5)$$

The frequency boundaries  $f_{\min}$  and  $f_{\max}$  correspond to the boundary respiratory rates of the HP-band, i.e. 6 breaths/min and 180 breaths/min, respectively.

**2) Best SQI:** The second approach consists in selecting the RR of the ROI with the highest SQI.

**3) Bayesian Fusion:** The Bayesian fusion is based on the well-known Bayes' law, which allows the estimation of a system state variable  $x$  (posterior probability distribution) using observations (measurements) from different sensors (ROIs in this case)  $s$ . In order to apply Bayesian fusion to the presented algorithm, current observations  $s_t^m$  (current analysis window) needed to be separated from previous observations  $s_{t-1}^m$

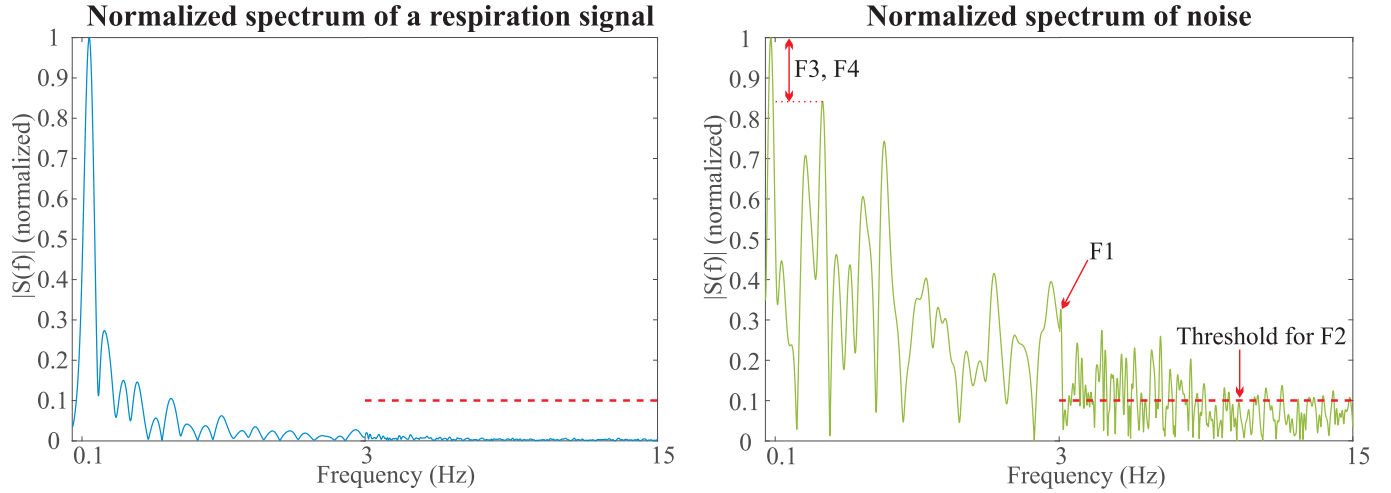


Fig. 2. Left: normalized spectrum of a representative respiratory signal resulting in a SQI of 0.98. Right: normalized spectrum of noise (SQI = 0.71) with features for SQI depicted. For better visualization of the LP- and BP-band, the frequency axes have been scaled.

(previous analysis windows):

$$p(\mathbf{x}|\mathbf{s}_t^m) = \frac{p(\mathbf{s}_t^m|\mathbf{x}, \mathbf{s}_{t-1}^m) \cdot p(\mathbf{x}|\mathbf{s}_{t-1}^m)}{p(\mathbf{s}_t^m|\mathbf{s}_{t-1}^m)}. \quad (6)$$

While  $p(\mathbf{s}_k^m|\mathbf{x}, \mathbf{s}_{k-1}^m)$  is the likelihood function,  $p(\mathbf{x}|\mathbf{s}_{k-1}^m)$  denotes the prior distribution. The denominator  $p(\mathbf{s}_k^m|\mathbf{s}_{k-1}^m)$  is a normalization factor for integrating the probability density function to one. The  $m$  available sensors (ROIs)  $s^1 \dots s^m$  are denoted by  $\mathbf{s}^m$ . In this work, we considered the sensors to be independent from each other, therefore

$$p(\mathbf{s}_k^m|\mathbf{x}, \mathbf{s}_{k-1}^m) = \prod_{i=1}^m p(s_k^i|\mathbf{x}, s_{k-1}^i). \quad (7)$$

Under this assumption, the Bayesian fusion can be calculated according to

$$p(\mathbf{x}|\mathbf{s}_k^1 \dots \mathbf{s}_k^m) = p(\mathbf{x}|\mathbf{s}_{k-1}^1 \dots \mathbf{s}_{k-1}^m) \cdot \prod_{i=1}^m \frac{p(\mathbf{x}|\mathbf{s}_k^i)}{p(\mathbf{x}|\mathbf{s}_{k-1}^i)}. \quad (8)$$

In this work, the system state variable  $\mathbf{x}$  stands for the RR and  $[\mathbf{s}_k^1 \dots \mathbf{s}_k^m]$  represents the RR of each valid ROI. Based on the probability function after Bayesian fusion, the RR was defined as the RR with the highest probability within the frequency boundaries of the BP-band (6 breaths/min and 180 breaths/min):

$$RR_{\text{fus}} = \arg \max p(\mathbf{x}|\mathbf{s}_k^1 \dots \mathbf{s}_k^m), RR_{\text{min}} \leq RR_{\text{fus}} \leq RR_{\text{max}}. \quad (9)$$

The analysis window was updated in steps of 1 second resulting in a temporal resolution of 1 Hz for the RR.

### III. EXPERIMENTAL PROTOCOL AND SETUP

The first aim of this work was to validate the feasibility of the proposed “black-box” algorithm. To achieve this, data of healthy volunteers collected in a previous study [31] were used. The second aim was to examine the capability of our approach to accurately estimate RR in newborn infants. For that, a second study was carried out with newborns at the division of

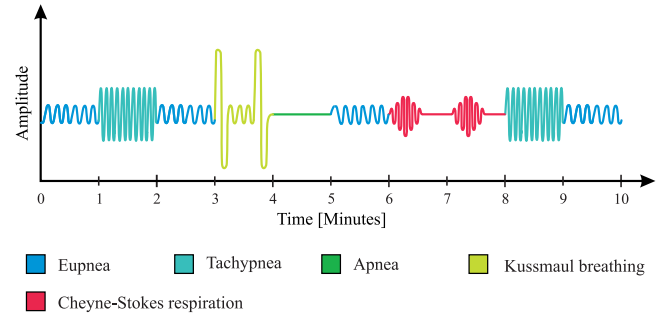


Fig. 3. Respiratory sequence simulated by the healthy volunteers in phase B. It consists of normal and altered breathing patterns: tachypnea, apnea, Kussmaul breathing and Cheyne-Stokes respiration.

Neonatology of the Sophia Children’s Hospital (Erasmus MC, Rotterdam, Netherlands).

#### A. Study in Healthy Subjects

Twelve healthy subjects (5 females and 7 males), between the ages of 21 and 31 ( $25.25 \pm 2.83$  years) voluntarily accepted to participate in the study. During the experiments, a long-wavelength infrared (LWIR) camera [VarioCAM® HD head 820S/30 mm (InfraTec GmbH, Dresden, Germany)] was sat atop a tripod located 2 m away from the subjects and at their height. The thermal camera has an uncooled infrared microbolometer focal plane array with a spatial resolution of  $1024 \times 768$  pixels and detects infrared wavelengths in the spectral range of  $7.5 \mu\text{m}$  to  $14 \mu\text{m}$ . At  $30^\circ\text{C}$ , its thermal sensitivity is better than  $0.05 \text{ K}$ . In addition, the thermal videos were acquired with a frame rate of 30 frames per second (fps).

The study protocol comprised two phases: A and B. In phase A, a nine minutes recording was carried out; the volunteers were instructed to sit still and breathe normally. In phase B, they were advised to simulate in a period of ten minutes the sequence represented in Fig. 3. It was composed of normal (eupnea) and diverse altered respiratory patterns (e.g. tachypnea, apnea, Kuss-

TABLE I  
PATIENT DATA

Infant	Gender	Gestational age [weeks + days]	Postnatal age [days]	Weight [g]	Sleeping position	Respiratory Support	Type of bed
I1	M	33 3/7	46	1705	Supine	O <sub>2</sub> therapy	Open bed
I2	M	33 3/7	46	1690	Lateral	O <sub>2</sub> therapy	Open bed
I3	F	32 6/7	29	1125	Prone	O <sub>2</sub> therapy	Incubator
I4	M	34 2/7	52	1850	Lateral	SIMV and PSV	Open bed
I5	M	27 3/7	6	950	Supine	CPAP	Incubator
I6	M	27 3/7	6	955	Supine	CPAP	Incubator
I7	F	40	26	3100	Supine	SIMV and PSV	Incubator
I8	M	30 2/7	3	1570	Lateral	CPAP	Incubator

**SIMV:** Synchronous Intermittent Mandatory Ventilation; **PSV:** Pressure Support Ventilation

**CPAP:** Continuous positive airway pressure

maul breathing and Cheyne-Stokes respiration). Thoracic effort (piezoplethysmography) was the ground truth (GT) used to validate the results. It was measured simultaneously with the data recording system SOMNolab 2 (Weinmann GmbH, Hamburg, Germany). In order to simplify signal synchronization, the volunteers were advised to hold their breath 15 s before beginning and 15 s after ending of each phase. The study design and protocol were approved by the Ethics Committee of RWTH Aachen University Hospital (EK 081/16).

### B. Study in Newborn Infants

To investigate the performance of the algorithms under real conditions, a feasibility study was carried out at the division of Neonatology of the Sophia Children's Hospital, Erasmus University Medical Center (Erasmus MC). Its design and protocol were approved by the Ethics Committee of the Erasmus MC (MEC\_2017-042). In order to be eligible to participate in this study, the subjects must meet all of the following criteria:

- 1) admitted to the Sophia Children's hospital;
- 2) gestational age between 24 and 42 weeks;
- 3) be in control of their breathing frequency (either non-invasive, synchronized, flow, or no respiratory support);
- 4) stable health condition.

Patients with time-dependent respiratory support were excluded from participation.

After obtaining informed consent from the parents/caregivers, two 5-minutes thermal recordings per patient (one on each side of the incubator/open bed) were carried out. For each recording of patients lying in incubators, a different door (left or right) was opened (note that it is not possible to record through the polycarbonate hood of the incubator due to its non-transparency for thermal radiation). When the patient was in an open bed, the curtain was slide aside slightly. The thermal camera [VarioCAM® HD head 820S/30 mm (InfraTec GmbH, Dresden, Germany)] was sat atop a tripod in front of the open door. As a matter of fact, patients were not moved for the recording, thus all sleeping positions were considered. Fig. 4 illustrates the study setup. In general, the observational study included eight newborn infants (6 males and 2 females) with the following characteristics: ges-



Fig. 4. Illustration of the study setup for an open bed.

tational age (GA)  $-32 \pm 4$  weeks, postnatal age (PA)  $-27 \pm 19$  days. Table I shows the patient data. To validate the results, the RR derived from body surface electrocardiography (ECG), measured with the M540 patient monitor (Dräger AG, Lübeck, Germany), was used. RR was acquired with a sampling rate of 1 Hz.

## IV. RESULTS

This section firstly describes the performance of our approach in thermal videos of healthy adult subjects (Section IV-A). Section IV-B, in turn, presents the results of the validation in newborn infants. The whole evaluation was performed in MATLAB (MATLAB 2017a, The MathWorks Inc., Natick, MA, USA).

### A. Study in Healthy Subjects

1) **Phase A:** Table II shows the performance of the algorithm for phase A. The best results were obtained using the fusion method *median*. The root-mean-square error (RMSE) hovered around  $(0.31 \pm 0.09)$  breaths/min. On average, 97.53% and 99.55% of the absolute errors did not transcend 1 breath/min and 2 breaths/min. By using the *best SQI*, similar results were

TABLE II  
PERFORMANCE OF THE APPROACH FOR PHASE A

Subject	Gender	Age	RMSE [breaths/min]		
			Median	best SQI	Bayes
S1	F	24	0.30	0.24	0.35
S2	F	24	0.27	0.24	0.79
S3	M	31	0.40	0.70	0.54
S4	M	27	0.38	0.39	0.34
S5	M	29	0.20	0.21	0.49
S6	M	25	0.22	0.22	0.34
S7	F	22	0.45	0.44	0.47
S8	M	25	0.47	0.47	0.56
S9	F	26	0.26	0.21	0.47
S10	M	26	0.20	0.20	0.56
S11	M	21	0.38	0.33	0.45
S12	F	23	0.24	0.22	0.79
Mean $\pm$ SD			0.31 $\pm$ 0.09	0.32 $\pm$ 0.15	0.51 $\pm$ 0.15

TABLE III  
PERFORMANCE OF THE APPROACH FOR PHASE B

Subject	RMSE [breaths/min]		
	Median	best SQI	Bayes
S1	2.36	2.27	2.70
S2	4.35	4.23	4.41
S3	3.17	3.19	3.26
S4	2.20	2.32	2.60
S5	2.49	2.46	2.75
S6	3.33	3.42	3.32
S7	4.36	5.34	4.18
S8	2.71	3.22	2.80
S9	3.63	3.78	3.67
S10	3.98	3.19	4.26
S11	2.96	3.01	3.04
S12	3.73	4.22	3.87
Mean $\pm$ SD	3.27 $\pm$ 0.72	3.39 $\pm$ 0.86	3.41 $\pm$ 0.63

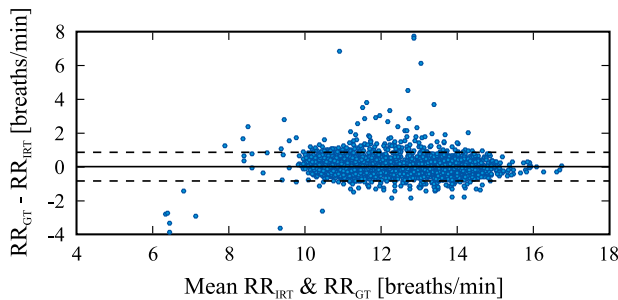


Fig. 5. Bland-Altman plot comparing both measurement methods, IRT ( $RR_{IRT}$ , fusion method median) and GT ( $RR_{GT}$ ). The bias averages 0.026 breaths/min (solid line) and the 95% limits of agreement vary between  $-0.82$  breaths/min and  $0.87$  breaths/min (dashed lines).

achieved; the RMSE averaged ( $0.32 \pm 0.15$ ) breaths/min. In addition, 97.82% and 99.53% of the absolute errors between both monitoring technologies (IRT and GT) were smaller than 1 breath/min and 2 breaths/min. Finally, with *Bayesian fusion* the RMSE was ( $0.51 \pm 0.15$ ) breaths/min. In comparison with the two previous fusion methods, the percentage of errors smaller than 1 breath/min and 2 breaths/min decreased to 92.19% and 99.39%, respectively. Additionally, the results showed similar mean correlation coefficients for the three fusion methods: 0.98 for both *median* and *best SQI*, and 0.95 for *Bayesian fusion* (all  $p$ -values were smaller than 0.05). Note, that the previous values were calculated by averaging the correlations calculated for each single subject.

Fig. 5 displays a Bland-Altman plot comparing both measurement techniques (IRT and GT). Using *median* for data fusion, a mean difference of 0.026 breaths/min was achieved and the limits of agreements ranged from  $-0.82$  breaths/min to  $0.87$  breaths/min.

2) **Phase B:** Table III shows, in turn, the performance of the algorithm for phase B. Also here, the best results were

obtained using the fusion method *median*; the RMSE hovered around ( $3.27 \pm 0.72$ ) breaths/min. On average, 88.60% of the absolute errors between IRT and GT did not exceed 2 breaths/min (81.09% were smaller than 1 breath/min). Using the *best SQI*, the following results were achieved: RMSE averaged ( $3.39 \pm 0.86$ ) breaths/min, and the absolute errors between both techniques were smaller than 1 breath/min and 2 breaths/min in 81.33% and 88.75% of the cases. Lastly, with the third fusion algorithm (*Bayesian fusion*), a RMSE of ( $3.41 \pm 0.63$ ) breaths/min was obtained. In this case, 79.76% and 88.82% of the absolute errors did not transcend 1 breath/min and 2 breaths/min. Also in phase B similar mean correlation coefficients were obtained for the three fusion methods: 0.95 for *median* and 0.94 for both *best SQI* and *Bayesian fusion* (all  $p$ -values were smaller than 0.05).

Fig. 6 shows the RR estimated with thermal imaging (solid blue line) as well as the GT signal (green dashed line). This illustrative example displays the signals correspond to subject S5 (phase B). In Fig. 7, a Bland-Altman plot comparing both monitoring techniques is presented. In this example, *median* was the method used for data fusion. In general, the Bland-Altman demonstrates a bias of 0.78 breaths/min and limits of agreement range from  $-6.4$  breaths/min to  $8.0$  breaths/min. Outliers are highlighted by the gray shading regions (more details in Section V - Discussion).

## B. Study in Newborn Infants

Table IV demonstrates the performance of the proposed algorithm for each infant and video sequence (1 and 2). Unfortunately, during the first video recording the infant I3 became agitated (due to reasons not related with this study). As the signals only contained movement artifacts, the sequence was not considered for evaluation. Using the *median* for signal fusion, a mean RMSE of ( $4.15 \pm 1.44$ ) breaths/min was obtained. In ad-

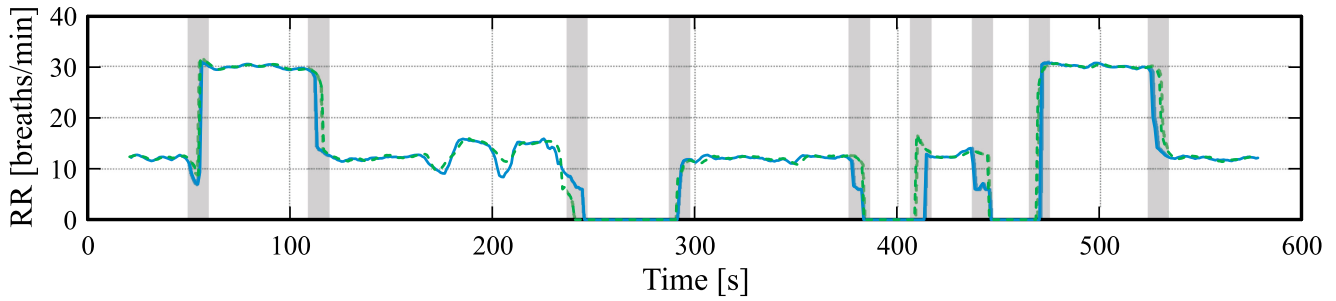


Fig. 6. Estimated RR correspondent to subject S5 (blue solid-IRT, green dashed line-GT). Median approach was used for data fusion. The gray shading regions show the transitions between different respiratory patterns.

TABLE IV  
PERFORMANCE OF THE APPROACH ON THERMAL VIDEOS OF NEWBORN INFANTS

Infant	Sequence	$RR_{GT}$ [breaths/min]	$RR_{IRT}$ [breaths/min]	RMSE [breaths/min]	$\bar{\epsilon}$ [breaths/min]	$\bar{\epsilon}_{90}$ [breaths/min]
I1	1	62.05	59.41	4.79	4.17	7.71
	2	53.86	51.2	6.11	5.16	8.96
I2	1	46.45	46.88	4.53	3.49	7.69
	2	50.24	52.86	6.75	5.14	11.68
I3	1	-	-	-	-	-
	2	47.49	46.99	4.29	3.43	6.86
I4	1	53.03	52.08	1.95	1.48	2.97
	2	55.63	56.07	1.53	1.15	2.97
I5	1	53.35	56.51	3.98	3.29	5.53
	2	49.6	47.96	2.86	2.42	4.59
I6	1	69.56	68.17	5.02	4.06	8.62
	2	61.84	62.35	5.91	5.31	8.83
I7	1	49.38	51.88	3.56	3.06	5.83
	2	49.91	51.34	2.67	2.02	4.58
I8	1	59.50	57.15	4.42	3.76	7.03
	2	51.02	50.96	3.86	2.44	4.09
Mean $\pm$ SD		$54.19 \pm 6.23$	$54.12 \pm 5.72$	$4.15 \pm 1.44$	$3.36 \pm 1.25$	$6.53 \pm 2.39$

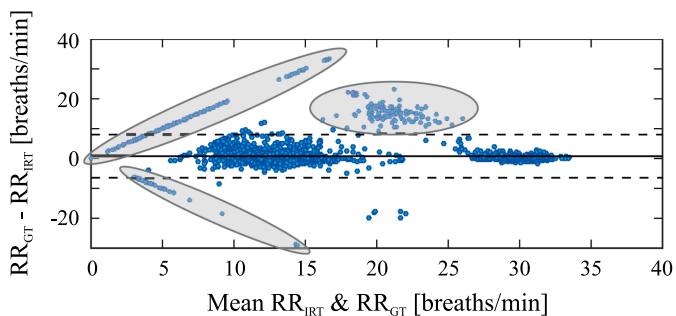


Fig. 7. Bland-Altman plot comparing both measurement methods, IRT ( $RR_{IRT}$ , fusion method median) and GT ( $RR_{GT}$ ). The bias averages 0.78 breaths/min (solid line) and the 95% limits of agreement vary between  $-6.4$  breaths/min and  $8.0$  breaths/min (dashed lines). Outliers are highlighted by the gray shading regions.

dition, the mean RR error ( $\bar{\epsilon}$ ) was  $(3.36 \pm 1.25)$  breaths/min and the spread of the error, calculated using the 90th percentile of the errors ( $\bar{\epsilon}_{90}$ ), reached  $(6.53 \pm 2.39)$  breaths/min. On average, the RR of the newborn infants hovered around  $(54.19 \pm 6.23)$  breaths/min. The results showed a mean correlation of 0.79 (all  $p$ -values were smaller than 0.05).

Fig. 8 depicts a Bland-Altman plot comparing both measurement techniques, IRT and GT. According to the results, the estimated mean difference was 0.24 breaths/min and the limits of agreement ranged from  $-8.1$  breaths/min to  $8.6$  breaths/min. Lastly, Fig. 9 shows the RR estimated with thermal imaging (solid line) as well as the GT signal (dashed line). This illustrative example displays the signals of infant I7 (video sequence 2).

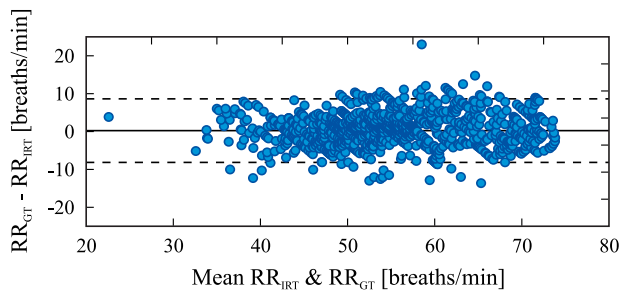


Fig. 8. Bland-Altman plot comparing both measurement methods, IRT ( $RR_{IRT}$ , fusion method median) and GT ( $RR_{GT}$ ). The bias averages 0.24 breaths/min (solid line) and the 95% limits of agreement vary between  $-8.1$  breaths/min and 8.6 breaths/min (dashed lines).

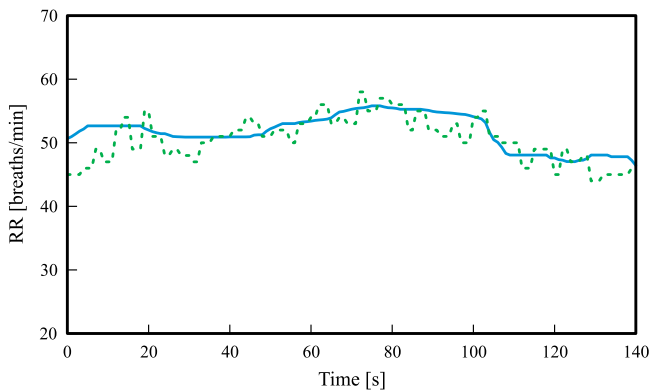


Fig. 9. Illustrative example showing estimated RR. Whereas the dashed line corresponds to the GT, the solid line stands for the RR estimated with IRT. The signals correspond to subject 17 (video sequence 2).

## V. DISCUSSION

Respiratory rate is a primary vital sign in critical care. However, it is also one of the major undocumented parameters. This is mainly due to the drawbacks of current monitoring techniques, which rely on cables as well as on the attachment of sensors. In neonatal care, cables and electrodes contribute significantly to stress and discomfort. Especially preterm and VLBW infants have a very thin and sensitive skin, thus adhesive electrodes often damage their skin when being removed. To overcome all these issues, scientists seek for new reliable and unobtrusive monitoring alternatives.

The current paper proposed a novel approach for noninvasive and passive assessment of RR in newborn infants using IRT. As a proof-of-concept, its performance was firstly validated in a study involving twelve healthy adult human subjects. Here, the robustness of the algorithm under challenging conditions (e.g. variable RR and simulated respiratory disorders) was investigated. A second study was carried out in eight newborn infants hosted in an incubator under real conditions.

### A. Study in Healthy Subjects

The presented approach was firstly validated using thermal videos of twelve healthy adults. In phase A (subjects were

advised to breath normally), a good agreement between GT (piezoplethysmography) and thermal imaging was observed. By using the *median* for sensor fusion, the best results were achieved, with a mean RMSE of  $(0.31 \pm 0.09)$  breaths/min. The Bland-Altman plot of Fig. 5 together with the mean correlation coefficient and the percentage of errors smaller than 1 and 2 breaths/min (92.19% and 99.39%) corroborate the good agreement between both monitoring technologies. To examine clinically relevant scenarios within the study, a wide range of physiological and pathological respiratory patterns (including eupnea, tachypnea, apnea, Kussmaul breathing, and Cheyne-Stokes respiration) were simulated in phase B. Table III together with the Bland-Altman plot of Fig. 7 show higher RR errors in Phase B (compare with Table II and Fig. 5 of phase A). In this phase, abrupt changes in RR were simulated (e.g. from 0 breaths/min to 30 breaths/min), as illustrated in Fig. 3 and Fig. 6. Therefore, small delays between GT and IRT in these transitions caused higher temporal errors, which negatively influenced the RMSEs displayed in Table III. These errors correspond to the outliers illustrated by the gray shading regions of Fig. 7. The great discrepancies occurred in transitions such as eupnea to tachypnea, tachypnea to eupnea, apnea to tachypnea, tachypnea to eupnea, etc. The previous statements together with Fig. 6 prove that the errors between IRT and GT outside these passages were actually quite small. Indeed, as described in Section IV-A, the percentage of absolute errors smaller than 1 and 2 breaths/min hovered around 81.09% and 88.60%, respectively. In addition, two techniques based on different measurement principles were compared, which may contributed to small lags or different reaction times in the transitions between distinct respiratory patterns.

In 2017, our group proposed another approach to estimate RR from thermal videos of adult volunteers [31]. Note that the video sequences were used in the current paper to test the feasibility of the “black-box” algorithm. The approach presented in 2017 used the information of four different ROIs to compute RR (“multiple regions of interest” approach): nose (temperature modulation), mouth (temperature modulation), and shoulders (movement). To measure RR, the ROIs were automatically identified in the first frame of the video sequence and, afterwards tracked. In a further step, the four respiratory waveforms were extracted. Lastly, the RR from the four ROIs were fused to minimize the detection error probability and to achieve a higher reliability. Despite of the good results, it presented a major drawback. For an automatic detection of all ROIs, the subjects must lay in supine position. To overcome this issue, we developed a novel algorithm, presented in this paper, which does not use any anatomical region to estimate RR; it regards thermal video sequences as black-boxes. In brief, similar results between the two approaches were obtained. By applying the “black-box” algorithm, a mean RMSE of 0.31 breaths/min and 3.27 breaths/min was obtained for phase A and B, respectively. Using the approach “multiple regions of interest”, the mean RMSEs averaged 0.28 breaths/min and 3.36 breaths/min. In sum, the results indicate that the proposed approach is capable of accurately estimating RR in thermal videos even during challenging conditions.

## B. Study in Newborn Infants

After a successful validation on thermal videos of healthy adults, the performance of the “black-box” algorithm was examined on data from newborn infants under incubator care. For the two recordings, the camera was placed first on the left and then on the right side of the medical device. One aim of the study was to discover whether the position of the infants affects the analysis technique. Thus, patients were not moved for video acquisition.

Table IV and the correlation analysis show the good agreement between the proposed method and reference, with a mean RMSE of  $(4.15 \pm 1.44)$  breaths/min and a mean correlation coefficient of 0.79. The Bland-Altman plot of Fig. 8 shows a very good accuracy (ability to measure RR close to its true value) between thermal imaging and GT as corroborated by the small bias (0.24 breaths/min). The 95% limits of agreement ( $-8.1$  breaths/min, 8.6 breaths/min), on the other hand, indicate a higher spread of the errors. There are some reasons that justify these higher errors. First, RR derived from ECG is very prone to motion artifacts, to physiologic events which induce thoracic movements unrelated to respiration (e.g. crying), and to poor ECG electrode placement. Second, the monitoring modalities as well as the algorithms (e.g. filtering, averaging) used to compute this vital parameter are different. Lastly, the RR from newborn infants varies constantly and is also characterized by abrupt changes. Therefore, small delays between thermal imaging and GT may lead to high errors.

In 2011, Abbas *et al.* [27] evaluated the capability of their approach to estimate RR in eight preterm neonates. This algorithm tracks a ROI enclosing the nose in order to detect temperature fluctuations during the respiratory cycle. Despite of the outstanding results, this approach is impracticable during respiratory support via face masks and it strongly depends on sleeping position, since the nostrils must be always in the field of view of the thermal camera. In our paper, we demonstrated that our algorithm is capable of detecting this vital parameter without being affected by the (1) sleeping position, (2) position of the head and (3) by the oxygen delivery method (e.g. face masks, nasal cannulae, nasal prongs).

The major drawback of the proposed algorithm is the sensitivity to motion artifacts. Therefore, the next aim should be to integrate a motion analysis algorithm capable of detecting motion noise inside the incubator, including patient movement, nursing interventions or maternal touch. In the clinical study, the recordings were performed with the door of the incubator opened, since its polycarbonate hood is not transparent for thermal radiation. In a real setting, the camera should be integrated inside of the incubator, or the setting proposed by Villarroel *et al.* [26] should be adopted, where a 3 cm hole was cut in the top of the incubator canopy.

Thermal imaging is still an expensive technology, especially when compared with other techniques, such as radar or visible imaging systems, which are relatively affordable. However, IRT has peculiar specifications that make it very attractive for diverse medical applications, especially in neonatology. First, thermal imaging is a passive technique, i.e. it measures the ra-

diation emanated by the body. In contrast, radar is an active system, which irradiates the patient with electromagnetic radiation. Regarding safety aspects and a future product approval, such characteristics are particularly valuable, as the eligibility criteria for neonatal medical equipment are very rigorous. Secondly, contrary to other technologies, thermal imaging is also capable of “seeing” in total darkness. Near-infrared and visible imaging systems, in turn, require at least a small amount of light to produce an image. Thus, a 24 hours monitoring would require an active radiation of the patients, at least during the night. Thirdly, IRT also allows the monitoring of body temperature and body temperature distribution.

Until a few years ago, thermal cameras were mostly used for military applications. Nevertheless, in the last decade, thermal imaging cameras are finding their way in more and more consumer-oriented applications, like driver vision enhancement and home security, leading to an increase in production volumes and, consequently, to a decrease in prices. As other technologies, we believe that IRT systems will become affordable, compact and, image quality will even further improve.

The calibration of an uncooled IRT camera is still a very complex process. Therefore, their use for applications that require a very accurate temperature measurement might not be meaningful. In our case, absolute accuracy is not a crucial parameter, since we do not intend to measure absolute temperatures. Instead of accuracy, a good thermal sensitivity and resolution is mandatory for RR assessment, since the acquired videos must have a good contrast.

## VI. CONCLUSION

Unobtrusive and non-contact monitoring of RR and other vital signs have become increasingly important during the last years. Doppler radar, magnetic impedance and camera technologies (visible, near-infrared, mid-wave infrared, and LWIR imaging systems) can be an important contribution to unobtrusive vital signs monitoring.

In this paper, a novel approach to unobtrusive and non-contact RR monitoring using a LWIR camera was presented. Instead of tracking anatomic landmarks, a grid of regions of interest was laid over the image and an algorithm was developed in order to automatically select ROIs suitable for detection of respiration. Such an approach enables to monitor RR independent of the subject’s position and anatomic landmarks in the camera’s field of view. In order to further improve accuracy, different methods were used to fuse the information available from the different ROIs.

Initially, the validation of the algorithm demonstrated its high accuracy compared to a clinical gold standard using data from a lab experiment. Afterwards, the algorithm was validated using clinical data recorded during a study with preterm neonates. Again, the algorithm showed very good results (mean RMSE of  $(4.15 \pm 1.44)$  breaths/min). In conclusion, this approach was able to robustly extract RR from LWIR video sequences not only in lab settings, but also under real clinical conditions. Therefore, IRT may be a very promising and clinically relevant alternative for current monitoring technologies in neonatal care.

## REFERENCES

- [1] A. C. Guyton and J. E. Hall, Eds., *Textbook of Medical Physiology*. 11th ed. Philadelphia, PA, USA: Saunders, 2006.
- [2] S. R. Braun, "Respiratory rate and pattern," in *Clinical Methods: The History, Physical, and Laboratory Examinations*, H. K. Walker, W. D. Hall, and J. W. Hurst, Eds., 3rd ed. Atlanta, GA, USA: Butterworths, 1990, ch. 43, pp. 226–230.
- [3] M. A. Cretikos *et al.*, "Respiratory rate: The neglected vital sign," *Med. J. Australia*, vol. 188, no. 11, pp. 657–659, 2008.
- [4] M. Elliott and A. Coventry, "Critical care: The eight vital signs of patient monitoring," *British J. Nursing*, vol. 21, no. 10, pp. 621–625, 2012.
- [5] A. D. Droitcour *et al.*, "Non-contact respiratory rate measurement validation for hospitalized patients," in *Proc. Annu. Int. Conf. IEEE Eng. Med. Biol. Soc.*, 2009, pp. 4812–4815.
- [6] A. Thomas and L. J. Maxwell, "Clinical assessment," in *Cardiorespiratory Physiotherapy: Adults and Paediatrics*, E. Main and L. Denehy, Eds., 5th ed. Amsterdam, The Netherlands: Elsevier, 2016, ch. 2.
- [7] J. P. Kowalak, Ed., *Lippincott's Nursing Procedures*. 5th ed. Baltimore, MD, USA: Williams & Wilkins, 2009.
- [8] W. Q. Lindh *et al.*, *Delmar's Comprehensive Medical Assisting: Administrative and Clinical Competencies*. Boston, MA, USA: Cengage Learning, 2013.
- [9] B. Yoost and L. Crawford, *Fundamentals of Nursing: Active Learning for Collaborative Practice*. 1st ed. St. Louis, MO, USA: Mosby, 2015.
- [10] D. C. Shellely and J. I. Peters, *Respiratory Care: Patient Assessment and Care Plan Development*. 1st ed. Boston, MA, USA: Jones&Bartlett, 2016.
- [11] T. Duning *et al.*, "Brainstem involvement as a cause of central sleep apnea: Pattern of microstructural cerebral damage in patients with cerebral microangiopathy," *PLoS One*, vol. 8, no. 4, 2013, Art. no. e60304.
- [12] M. M. Siccoli *et al.*, "Central periodic breathing during sleep in 74 patients with acute ischemic stroke-neurogenic and cardiogenic factors," *J. Neurol.*, vol. 255, no. 11, pp. 1687–1692, 2008.
- [13] R. L. Riha, "Diagnostic approaches to respiratory sleep disorders," *J. Thoracic Disease*, vol. 7, no. 8, pp. 1373–1384, 2015.
- [14] F. Olivier *et al.*, "Association between apnea of prematurity and respiratory distress syndrome in late preterm infants: An observational study," *Frontiers Pediatrics*, vol. 4, p. 105, 2016.
- [15] J. S. Tregoning and J. Schwarze, "Respiratory viral infections in infants: causes, clinical symptoms, virology, and immunology," *Clin. Microbiol. Rev.*, vol. 23, no. 1, pp. 74–98, Jan. 2010.
- [16] J. Fei and I. Pavlidis, "Virtual thermistor" in *Proc. IEEE Eng. Medicine Biol. Soc.*, vol. 2007, 2007, pp. 250–253.
- [17] F. McGain *et al.*, "Documentation of clinical review and vital signs after major surgery," *Med. J. Australia*, vol. 189, no. 7, pp. 380–383, 2008.
- [18] A. K. Abbas *et al.*, "Neonatal infrared thermography imaging: Analysis of heat flux during different clinical scenarios," *Infrared Phys. Technol.*, vol. 55, no. 6, pp. 538–548, Nov. 2012.
- [19] M. M. Baharestani, "An overview of neonatal and pediatric wound care knowledge and considerations," *Ostomy Wound Manage.*, vol. 53, no. 6, pp. 34–55, 2007.
- [20] J. M. Kuller, "Skin breakdown: Risk factors, prevention, and treatment," *Newborn Infant Nursing Rev.*, vol. 1, no. 1, pp. 35–42, 2001.
- [21] E. Greneker, "Radar sensing of heartbeat and respiration at a distance with applications of the technology," in *Proc. RADAR 97*, 1997, pp. 150–154. [Online]. Available: [http://digital-library.theiet.org/content/conferences/10.1049/cp\\_199\\_71650](http://digital-library.theiet.org/content/conferences/10.1049/cp_199_71650)
- [22] M. Steffen *et al.*, "Multichannel simultaneous magnetic induction measurement system \050MUSIMITOS\051," *Physiological Meas.*, vol. 29, no. 6, pp. S291–S306, Jun. 2008.
- [23] P. Marchionni *et al.*, "An optical measurement method for the simultaneous assessment of respiration and heart rates in preterm infants," *Rev. Scientific Instrum.*, vol. 84, no. 12, Dec. 2013, Art. no. 121705.
- [24] M. Bartula *et al.*, "Camera-based system for contactless monitoring of respiration," in *Proc. 35th Annu. Int. Conf. IEEE Eng. Med. Biol. Soc.*, 2013, pp. 2672–2675.
- [25] F. Zhao *et al.*, "Remote measurements of heart and respiration rates for telemedicine," *PLoS one*, vol. 8, no. 10, 2013, Art. no. e71384.
- [26] M. Villarreal *et al.*, "Continuous non-contact vital sign monitoring in neonatal intensive care unit," *Healthcare Technol. Lett.*, vol. 1, no. 3, pp. 87–91, Sep. 2014.
- [27] A. K. Abbas *et al.*, "Neonatal non-contact respiratory monitoring based on real-time infrared thermography," *BioMed. Eng. OnLine*, vol. 10, no. 93, pp. 1–17, 2011.
- [28] C. Barbosa Pereira *et al.*, "Remote monitoring of breathing dynamics using infrared thermography," *Biomed. Opt. Express*, vol. 6, no. 11, pp. 4378–4394, 2015.
- [29] C. B. Pereira *et al.*, "Contact-free monitoring of circulation and perfusion dynamics based on the analysis of thermal imagery," *Biomed. Opt. Express*, vol. 5, no. 4, pp. 1075–89, Apr. 2014.
- [30] G. F. Lewis *et al.*, "A novel method for extracting respiration rate and relative tidal volume from infrared thermography," *Psychophysiology*, vol. 48, no. 7, pp. 877–887, 2011.
- [31] C. Barbosa Pereira *et al.*, "Estimation of breathing rate in thermal imaging videos: a pilot study on healthy human subjects," *J. Clinical Monitoring Comput.*, vol. 31, no. 6, pp. 1241–1254, Dec. 2017.
- [32] C. Pereira *et al.*, "Estimation of respiratory rate from thermal videos of preterm infants," in *Proc. Annu. Int. Conf. IEEE Eng. Med. Biol. Soc.*, 2017.
- [33] J. Jorge *et al.*, "Data fusion for improved camera-based detection of respiration in neonates," in *Proc. Optical Diagnostics and Sensing XVIII: Toward Point-of-Care Diagnostics*, vol. 10501, 2018.
- [34] D. Fergusson, "Respiratory assessment," in *Clinical Assessment and Monitoring in Children*, D. Fergusson, Ed., 1st ed. Oxford, U.K.: Blackwell Publishing, 2008, ch. 2.
- [35] R. M. Insoft and I. D. Todres, "Growth and development," in *A Practice of Anesthesia for Infants and Children*, C. J. Coté, J. Lerman, and I. D. Todres, Eds., 4th ed. Philadelphia, PA, USA: Saunders, 2009, ch. 2.